pubs.acs.org/acschemicalbiology

Articles

Fluorogenic RNA-Based Biosensor to Sense the Glycolytic Flux in Mammalian Cells

Ignazio Geraci, Alexis Autour, Georg Pietruschka, Aleksandra Shiian, Marina Borisova, Christoph Mayer, Michael Ryckelynck, and Günter Mayer*

Cite This: *ACS Chem. Biol.* 2022, 17, 1164–1173

Read Online

ACCESS | Metrics & More | Article Recommendations | Supporting Information

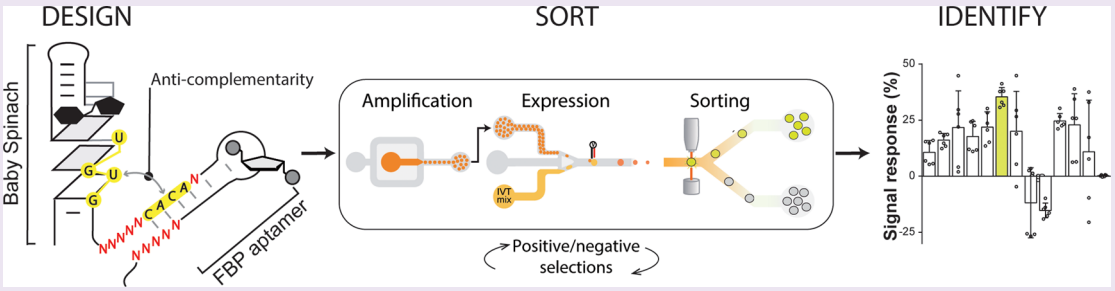

ABSTRACT: The visualization of metabolic flux in real time requires sensor molecules that transduce variations of metabolite concentrations into an appropriate output signal. In this regard, fluorogenic RNA-based biosensors are promising molecular tools as they fluoresce only upon binding to another molecule. However, to date no such sensor is available that enables the direct observation of key metabolites in mammalian cells. Toward this direction, we selected and characterized an RNA light-up sensor designed to respond to fructose 1,6-bisphosphate and applied it to probe glycolytic flux variation in mammal cells.

Fructose 1,6-bisphosphate (FBP) is a key metabolite found to be consistent with glycolytic flux in bacteria,[1] yeast,[2] and mammalian cells.[3] Molecular tools that detect FBP levels in mammalian cells and in real time are highly demanded but remain elusive.[4] Fluorogenic RNA-based biosensors have emerged as promising tools and are meant to fill this gap in visualizing the presence and absence of or dynamic changes in the concentration of distinct molecules, for example, microRNA,[5] proteins,[6] and metabolites.[7−10] These RNA devices are built from a light-up RNA molecule[11−14] that is allosterically conjoined to a second aptamer domain interacting with a molecule of choice.[15,16] However, attaining allosteric control is not yet generalizable, and each light-up device requires an iterative process of design and testing to gain appropriate regulation. Currently available sensors that detect metabolites are restricted to the use of aptamer domains from natural riboswitches, for example, *S*-adenosyl methionine or thiamine pyrophosphate (TPP).[10,15]

Here, we report on the identification of an RNA device that upon expression in HEK293T cells responds to oligomycin A, a well-known glycolytic booster.[3,17,18] This sensor was built from an in vitro selected aptamer that binds FBP and the light-up RNA Baby Spinach, which binds to DFHBI.[19] We employed an allosteric design-selection approach by generating a library of ∼4 million different sequences that was subjected to a microfluidic-assisted in vitro compartmentalization (μIVC)[20,21] process to identify RNA sensors able to fluoresce only upon FBP recognition. This process was found to outcompete a conventional in vitro selection method (SELEX)[22] that we also pursued, which relied on affinity separation to identify a light-up FBP sensor.

RESULTS AND DISCUSSION

Initially, in our attempt to identify RNA molecules that allosterically bind to DFHBI, depending on the specific target molecule interaction, we used a stem loop structure bearing library, previously employed to identify the DFHBI-binding RNA aptamer Spinach.[12] In this selection, scheme target-independent DFHBI binders were depleted by a negative selection step, in which an RNA library was incubated with DFHBI coupled to sepharose beads prior to a target-dependent selection step (Supporting Information, Figure 1a). We applied this scheme to four different target molecules, that is, acetyl CoA, FBP, lysozyme, and miR21. Selection experiments using the latter three compounds did not yield the enrichment of DFHBI-binding sequences, whereas acetyl CoA was found to enable enrichment but in a target independent

Received: February 6, 2022
Accepted: April 6, 2022
Published: April 15, 2022

https://doi.org/10.1021/acschembio.2c00100
ACS Chem. Biol. 2022, 17, 1164–1173

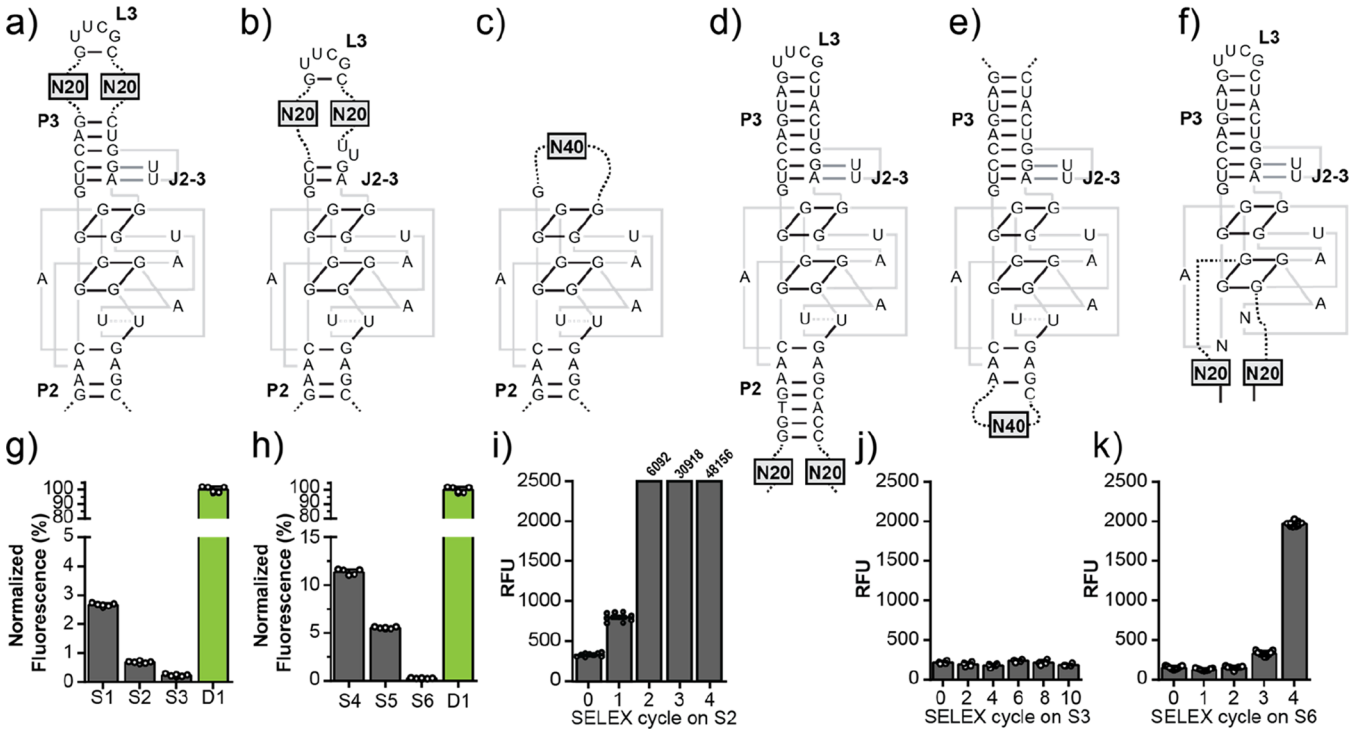

Figure 1. S6 chosen as a partially structured library of Baby Spinach. (a−f) Structurally driven design of Baby Spinach libraries, in which the sequences supporting the G-quadruplex folding were progressively randomized from the stems P3 [S1−3 (a−c)] and P2 [S4−6 (d−f)] sides. (g,h) Background fluorescence measurement of DFHBI binders within the libraries S1 to S3 (d) and S4 to S6 (h), normalized to the D1 aptamer control, which was set to 100%. (i−k) Test DFHBI SELEX of library S2 (i), S3 (j), and S6 (k). As for S2, the numerical values after cycle 2 indicate the average fluorescence. Assays were performed at 1 μM purified RNAs and 10 μM DFHBI in the selection buffer (125 mM KCl, 5 mM $MgCl_2$ in 40 mM HEPES pH 7.5).

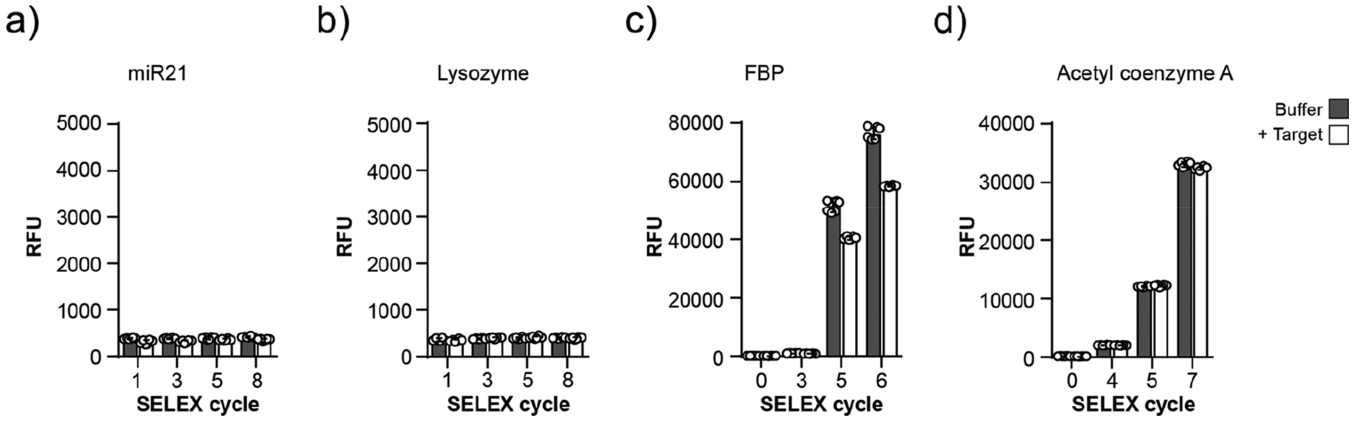

Figure 2. Allosteric SELEX on the S6 library for different ligands. Fluorescence binding analysis of different SELEX cycles on library S6 measured in the absence (gray) or presence (white) of miR21 [1 μM (a)] and lysozyme [0.2 μM, (b)], FBP [5 mM (c)] and AcCoA [200 μM (d)]. Assays were performed at 1 μM purified RNA and 10 μM DFHBI in the selection buffer (125 mM KCl, 5 mM $MgCl_2$ in 40 mM HEPES pH 7.5).

manner (Supporting Information, Figure 1b−e). In contrast, control selection experiments, aiming at identifying DFHBI binders, were performed successfully within five selection cycles (Supporting Information, Figure 2). Sequence analysis of this enriched library identified an aptamer resembling the previously identified variant of the Spinach aptamer—namely, Baby Spinach[23] (BS)—which we dubbed D1 (Supporting Information, Figures 3 and 4).

Having shown that a naïve RNA library was not capable of enriching allosteric RNA aptamers, we next designed a panel of structurally defined libraries based on the crystal structure of Spinach.[19] In these, the stem structures supporting BS's G-quadruplex formation were systematically randomized, that is, the P3 stem (in libraries S1−3, Figure 1a−c) and the P2 stem (in libraries S4−6, Figure 1e−g). In these libraries, the DFHBI-binding properties, measured by fluorescence intensity when incubating the RNA with DFHBI, correlate with the extent of BS randomization. The highest fluorescence was obtained with libraries S1 and S4 (11 and 3% compared to BS, respectively, Figure 1d,h) in which BS was less randomized. The fluorescence properties progressively dropped in libraries S2 and S5 (5 and <1%, Figure 1d,h) and was found to be below 1% in libraries S3 and S6 (Figure 1d,h). Libraries with high intrinsic fluorescence (S1, S4, and S5) properties were not

https://doi.org/10.1021/acschembio.2c00100
ACS Chem. Biol. 2022, 17, 1164−1173

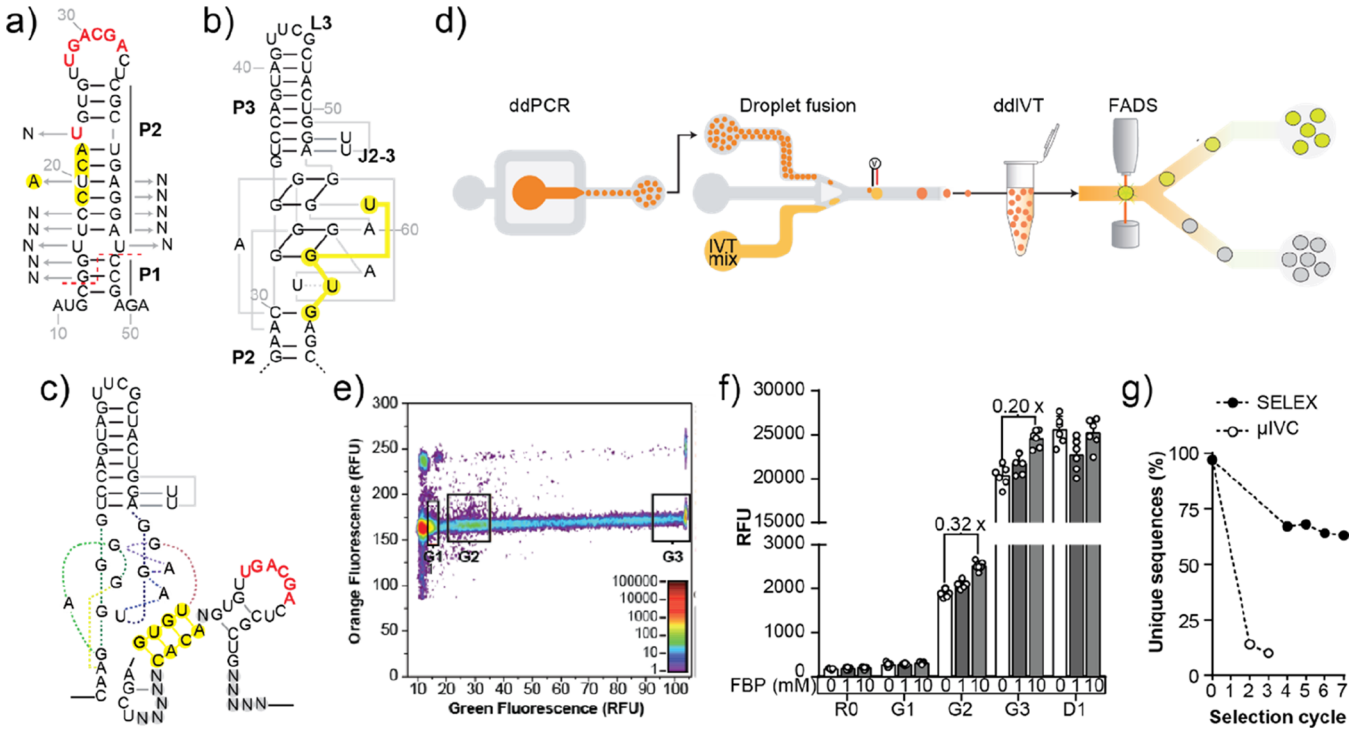

Figure 3. Screening of an FBP-responsive RNA biosensor using μIVC. (a) Secondary structure of the FBP-binding RNA aptamer C45.[25] The nucleotides exhibiting a reactivity pattern variation for 1-methyl-6-nitroisatoic anhydride (1M6) in SHAPE analysis are highlighted in red. Nucleotide U20 was substituted by an adenine to obtain a four-nucleotide stretch (nts 19−22, highlighted in yellow) anticomplementary to critical nucleotides of the Baby Spinach G-quadruplex domain [nts 62−65, highlighted in yellow (b)]. To design the chimeric library, C45 aptamer was shortened (red dotted line), and 10 nucleotides from the base of C45 stems P1 and P2 were randomized alongside nucleotide U23. (c) Structural representation of the chimeric RNA library, where the anticomplementary stretch between C45 and Baby Spinach aptamers is highlighted (yellow). (d) μIVC workflow to screen RNA-based biosensors responsive to FBP. Each gene contained in the library was individualized and amplified by limited dilution and droplet digital PCR (ddPCR). Each PCR droplet was then fused with in vitro transcription (IVT) mix droplet and incubated at 37 °C for 1 h to allow T7 transcription to occur (ddIVT). Finally, droplets were screened based on their fluorescence output with fluorescence-activated droplet sorting (FADS). (e) FADS profile of the third screening round of the chimeric library. Droplets resulting from 1:1 fusion between PCR and IVT droplets were identified thanks to the orange fluorescence (150−175 RFU) of Texas-Red added to each mixture; then, the droplets were gated by DFHBI-1T green fluorescence according to their fluorescence readout: G1 (15−17 RFU), G2 (22−35 RFU), and G3 (93−113 RFU). (f) FBP-dependent fluorescence induction of the sorted library pools obtained from gates G1−G3 (e) compared to the unenriched library (R0) and D1 aptamer (D1) at increasing concentrations of FBP in the μIVC buffer and 1 μM RNA. The FBP-dependent fold change is indicated as a numeric value. (g) NGS analysis indicated a drop of unique sequences in the gated RNA pools 0, 2, and G2 of cycle 3 (3) compared to the allosteric SELEX on the chimeric library.

further considered, as we assumed it would be unlikely to enrich allosteric binders in these. The three remaining libraries (S2, S3, and S6) were subjected to a DFHBI SELEX protocol (corresponding to the one described in the Supporting Information, Figure 2) to study their property in enriching DFHBI binders. These selection experiments revealed S2 and S6 being capable of enriching DFHBI-binding molecules, whereas S3 did not (Figure 1i−k). S2 and S6 reveal enriched DFHBI binders in selection cycles 3 and 4, respectively, whereas we anticipated that S6 might be best suited among the tested libraries for allosteric selection protocols. In S6 Spinach's stem, P2 and the mixed tetrad supporting the G-quadruplex formation were pointedly randomized to achieve low fluorescence of the library in the presence of DFHBI but retain the capability to enrich DFHBI binders (Figure 1k). We therefore used S6 in an allosteric selection scheme using miR21, lysozyme, acetyl-CoA, and FBP as target molecules (Figure 2). Similar to the results obtained when using the stem structure library (Supporting Information, Figure 1), no enrichment was observed using miR21 and lysozyme. Although DFHBI binders were enriched using acetyl-CoA and FBP, neither of the enriched libraries revealed target-dependent binding to DFHBI (Figure 2).

Because a generalized approach to identify allosteric binders of DFHBI for a target of choice was not successful, we next investigated the identification of an FBP sensor by emulating rational designs of conjoined aptamer modules.[15,16] We thus created a chimeric RNA library based on the light-up RNA Baby Spinach[23] and the aptamer C45.[24] C45 is a 51-nucleotide (nt) in vitro selected RNA aptamer that binds to FBP with a K_D-value of 6.5 ± 2.6 mM (Figure 3a).[24,25] Selective 2′-hydroxyl acylation analyzed by primer extension (SHAPE) revealed FBP-dependent variations in the reactivity pattern toward 1-methyl-6-nitroisatoic anhydride (1M6) of the bulged uridine (U23) in the P2 stem and of the nucleotides residing in the distal loop (nts 28−34) of C45 (Figure 3a).[25] Based on these data, we created a library that conjoins Baby Spinach with C45 and in which the critical nucleotides in the distal loop are maintained (Figure 3a), whereas in the stems, P1 and P2 nucleotides were randomized. Additionally, U20 in the P2 stem was exchanged for an adenine residue, thereby generating a four-nucleotide stretch (residues 19−22, CACA) that is complementary to the residues 62−65 (UGUG) of Baby

https://doi.org/10.1021/acschembio.2c00100
ACS Chem. Biol. 2022, 17, 1164−1173

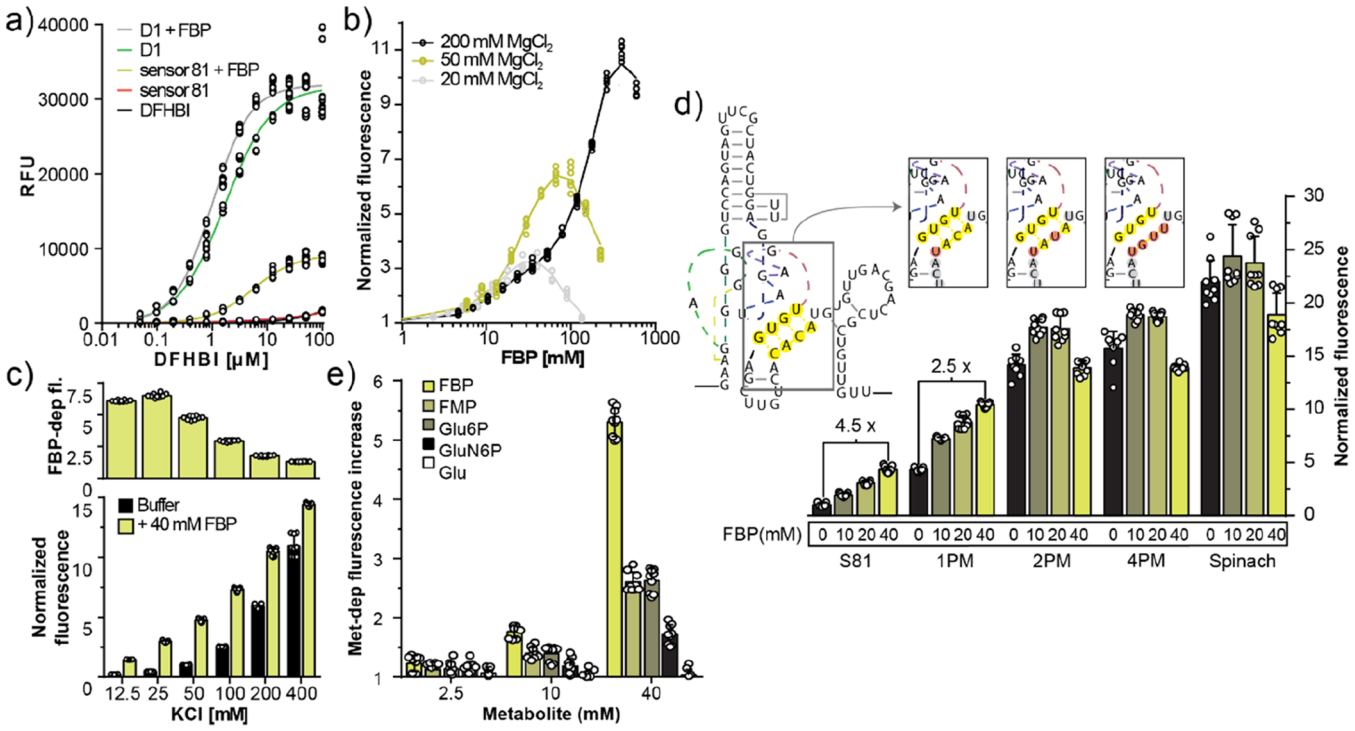

Figure 4. In vitro characterization of the FBP sensor 81. (a) EC_{50} measurement of s81 for DFHBI in the presence/absence of the maximal detectable concentration of FBP (250 mM) and compared to the D1 aptamer and DFHBI autofluorescence. Assay performed with 1 μM RNA in 40 mM Tris-HCl pH 7.9, 50 mM KCl, and 200 mM $MgCl_2$. Fluorescence intensity measured as RFU. (b) $MgCl_2$ dependency of s81 fluorescence response to FBP. Values are normalized to the background fluorescence of s81 without FBP, which was set to 1. (c) Impact of K^+ ions on the fluorescence detection of FBP by s81. At increasing concentrations of KCl, the fluorescence readout was measured in the absence of (black) and at 40 mM (yellow) FBP, and values were normalized, setting to 1 the background fluorescence of s81 at 50 mM KCl (bottom). The FBP-dependent fluorescence induction was calculated as the fold change incremental in each condition (top). (d) Point mutation analysis of s81 CACA stretch. The modified nucleotides in each mutant are highlighted in red. The fluorescence readout was measured at 1 μM RNA and 10 μM DFHBI in 40 mM Tris-HCl pH 7.9, 50 mM KCl, and 30 mM $MgCl_2$. Values were normalized, setting to 1 the background fluorescence of s81 without FBP. (e) Specificity response of s81 to a panel of metabolites similar to FBP. Fluorescence emission of sensor 81 with 2.5, 10, and 40 mM of fructose 1,6-bisphosphate (FBP), fructose 6-phosphate (F6P), glucose 6-phosphate (Glc6P), glucosamine 6-phosphate (GlcN6P), and glucose (Glc) and normalized to the Baby Spinach fluorescence variation with the different metabolites. Values were normalized to the background fluorescence of s81 and to the unspecific fluorescence variation of aptamer D1 with the different metabolites, which were both set to 1. The fluorescence readout was measured at 1 μM RNA and 10 μM DFHBI in 40 mM Tris-HCl pH 7.9, 50 mM KCl, and 30 mM $MgCl_2$. Data represent n = 3 independent experiments ± SD.

Spinach's G-quartet (Figure 3a,b). We hypothesized that, in the absence of FBP, the CACA stretch of C45 might interfere with G-quartet formation of Baby Spinach,[23] hence impairing its interaction with DFHBI. The stem P1 and parts of P2 that are required for FBP[25] were substituted by two stretches of five randomized nucleotides, of which one connected the two RNA aptamers. We additionally randomized the bulged U23, adjacent to the CACA stretch of C45 (Figure 3a,c), which showed a strong variation in the reactivity pattern in SHAPE but is inessential for FBP interaction.[25] This chimeric library has 11 random nucleotides, covering a sequence space of ~4 × 10^6 variants.

To enrich for FBP-dependent DFHBI binders, the chimeric library was also subjected to the allosteric SELEX scheme (Supporting Information, Figure 1). However, this approach yielded truncated by-products[24] dominating the enriched libraries (Supporting Information, Figure 5), which we were unable to overcome by RNA excision and purification from Urea-PAGE. Library truncation was also eminent by next-generation sequencing (NGS) analysis of the enriched pool (Supporting Information, Figure 5c). Although the libraries showed an increase in FBP-dependent fluorescence (Supporting Information, Figure 5a), the most enriched sequences from this approach did not (Supporting Information, Figure 5d). The percentage of unique sequence was still high (63%) in the RNA population from selection cycle 7 (Figure 3g), but due to the occurrence of the truncated by-products, additional selection cycles cannot be performed. Of note, the nucleotide distribution analysis of the enriched libraries seemed to reveal an increase in diversity, even in the constant regions (Supporting Information, Figure 6), indicative of pool degeneracy likely to compromise its overall function.

Based on these results, we decided to move toward the use of a microfluidic-assisted in vitro compartmentalization (μIVC) pipeline that allows us to sort single RNA species based on their fluorescence capacity under controlled conditions[20,21] (Figure 3d). To note, the diversity of the library matched the upper limit of the current μIVC procedure (up to 4 million droplets processed per round) and was expected to allow each sequence permutation to be analyzed.[26] Among other advantages, μIVC prevents rapid diffusion of a parasite within a population due to reaction compartmentalization and the elimination of parasite-containing droplets (decreased fitness).[27] We performed two initial rounds of screening in the presence of FBP to enrich the library in sequences prone to fluoresce (Supporting Information, Figure

https://doi.org/10.1021/acschembio.2c00100
ACS Chem. Biol. 2022, 17, 1164−1173

7). A third round was performed in the absence of FBP, and the droplets were gated displaying nil (G1), dim (G2), or high fluorescence (G3) (Figure 3e). In this way, we separated the non-fluorogenic RNAs (G1) and those displaying an FBP-independent fluorescence (G3) from FBP-dependent fluorescing species (G2, Figure 3e). Likewise, the G2-gated RNA population revealed the highest FBP-dependent increase in fluorescence (0.32-fold) compared to G1- and G3-gated populations (Figure 3f).

Next, we analyzed the G2-gated RNA population by NGS and Sanger sequence analysis (Supporting Information, Table 1), which revealed a co-enriched family of truncated RNA molecules that lost the region covering the first five random nucleotides up to nucleotide N23 and likely lost their capacity to interfere with Baby Spinach's DFHBI-binding ability. Besides them, sequences that reflected full-length RNA were identified, although no sequence revealed high copy numbers (Supporting Information, Table 1b). Interestingly, this persistence of full-length together with a reduced degeneration of constant sequences (Supporting Information, Figure 8) also pointed at the contribution of compartmentalization in protecting the system from unwanted events (e.g., recombination during PCR and parasite dissemination). The top-three full-length RNA candidates were the sequences X (0.75%), 85 (0.74%), and 86 (0.54%). Of note, 85 and 86 were also identified by Sanger sequencing. We chose these 3 and 14 other sequences and tested them for FBP-dependent fluorescence (Supporting Information, Figure 9). Candidates were initially ranked based on the fluorescence emission intensity and signal reliability with FBP in selection buffer, which included all components of the in vitro transcription reaction (Supporting Information, Figure 9a,b). The top 5 candidates (53, 63, s81, 85, and X) were subsequently tested in minimal Tris-KCl buffer to ascertain that the light-up properties of the candidates were not dependent on the buffer components, such as nucleotides or T7 RNA polymerase (Supporting Information, Figure 9c,d). Among all sequences, s81 exhibited the strongest fold-change of fluorescence (89% fluorescence increase when 10 mM FBP are added) in the presence of FBP and was chosen for further characterization.

Furthermore, s81 was found to be a low-copy number sequence (Supporting Information, Tables 2 and 3) in an optimized NGS deep-sequencing analysis, where full-length sequences were mined to bypass the enrichment of the shortened sequence family (Supporting Information, Figure 10). Nonetheless, s81 was identified as a reoccurring motif by the MEME suite[28] analysis of the top 50 sequences in the enriched pool 3.G2 (Supporting Information, Figure 11). A comparative analysis of the previously tested sensor candidates (Supporting Information, Figure 12) identified s81 as the sequence with the highest similarity to the paternal C45 aptamer (6 nt overlap of the random region; Supporting Information, Figure 12). Therefore, while s81 experienced low enrichment in the selection, its superior performance in the FBP-response assay compared to other sensor candidates could be explained by a balance between newly selected nucleotides and, on the other hand, a close similarity to the paternal C45 aptamer.

We investigated the concentration-dependent binding of s81 to DFHBI in the presence and absence of FBP (Figure 4a). Without FBP, the fluorescence of the sensor was found to be in the range of the fluorescence of DFHBI in the absence of Baby Spinach. In the presence of FBP, a concentration-dependent interaction with DFHBI was observed and an EC_{50} value of 5.56 ± 0.40 μM was determined, which is 3.5-fold and 4.9-fold higher compared to the EC_{50} values detected when using Baby Spinach in the absence (EC_{50} value of 1.61 ± 0.10 μM) or presence (1.13 ± 0.07 μM) of FBP, respectively. The overall fluorescence of s81 was found to be 3.3-fold less intense compared to Baby Spinach, as expected for a transiently destabilized aptamer.

Ortega et al. analyzed the in vitro binding affinity of aptamer C45—from which s81 derives its FBP binding module—and determined the aptamer's affinity to be in the millimolar range and to depend on the presence of mono- and divalent cations.[25] Thus, we next investigated the impact of K^+ and Mg^{2+} ions on sensor performance. K^+ ions are critical for the folding of Baby Spinach's G-quartet,[23] whereas Mg^{2+} ions are required by both aptamers to bind DFHBI or FBP, respectively.[23,25] FBP, however, is capable of binding to Mg^{2+} ions by itself,[27] therefore counteracting on sensor performance. This was evident from the variation in the detected fluorescence intensities of s81 at distinct amounts of Mg^{2+} ions but increasing FBP concentrations (Figure 4b). For example, at 20 mM Mg^{2+}, the maximal fluorescence intensity was obtained at 27 mM FBP. A further increase in the FBP concentration diminished the fluorescence signal, most likely due to Mg^{2+} deprivation. Likewise, increasing the concentration of Mg^{2+} resulted in a stronger fluorescence signal with the maxima shifted to higher FBP concentrations (Figure 4b). In turn, increasing the concentration of K^+ ions results in a loss of FBP dependence but overall higher fluorescence intensities of s81 (Figure 4c). K^+ ions stabilize Baby Spinach's G-quartet[23] and therefore counterbalance the FBP dependence of s81, indicating that its allosteric control is based on the G-quartet destabilization.

To further confirm that the initial library design is maintained in s81, we designed a series of mutants of the CACA region meant to weaken its hybridization to the residues 62−65 UGUG of Baby Spinach's G-quartet (Figure 4d). Of note, the fluorescence in the absence of FBP increased with the increase in the degree of destabilization and reached the fluorescence of Baby Spinach when all 4 nucleotides were mutated (4PM, Figure 4d). Specifically, a single-point mutation in the CACA region (1PM) was found to diminish the performance of the sensor, and additional mutations (2PM, 4PM) lead to a complete loss of allosteric control (Figure 4d). Taken together, these data indicated that, according to the initial design strategy, the CACA region of s81 is important for the transduction of FBP binding.

Next, we examined the specificity of the sensor for a panel of metabolites related to FBP (Figure 4e). The highest light-up rate of the sensor was observed in the presence of FBP (1.2-, 1.8-, and 5.3-fold at increasing FBP) and was twice more specific for FBP than for related metabolites, that is, fructose monophosphate (F6P) and glucose-6-phosphate (Glc6P) (1.1-, 1.4-, and 2.6-fold, respectively). Of note, F6P and Glc6P are metabolic precursors of FBP in glycolysis, but conversely to FBP, they have been reported to not vary upon the glycolytic flux fluctuation in mammalian cells.[3]

To validate if s81 was capable of sensing changes in the FBP concentration in cells, we expressed it in HEK293T cells using the Tornado expression system, based on a re-engineered version of the Φ29 scaffold named F30 that allows the expression of RNAs as a stable circular construct.[29] First, we confirmed that the light-up FBP induction was not affected by

https://doi.org/10.1021/acschembio.2c00100
ACS Chem. Biol. 2022, 17, 1164−1173

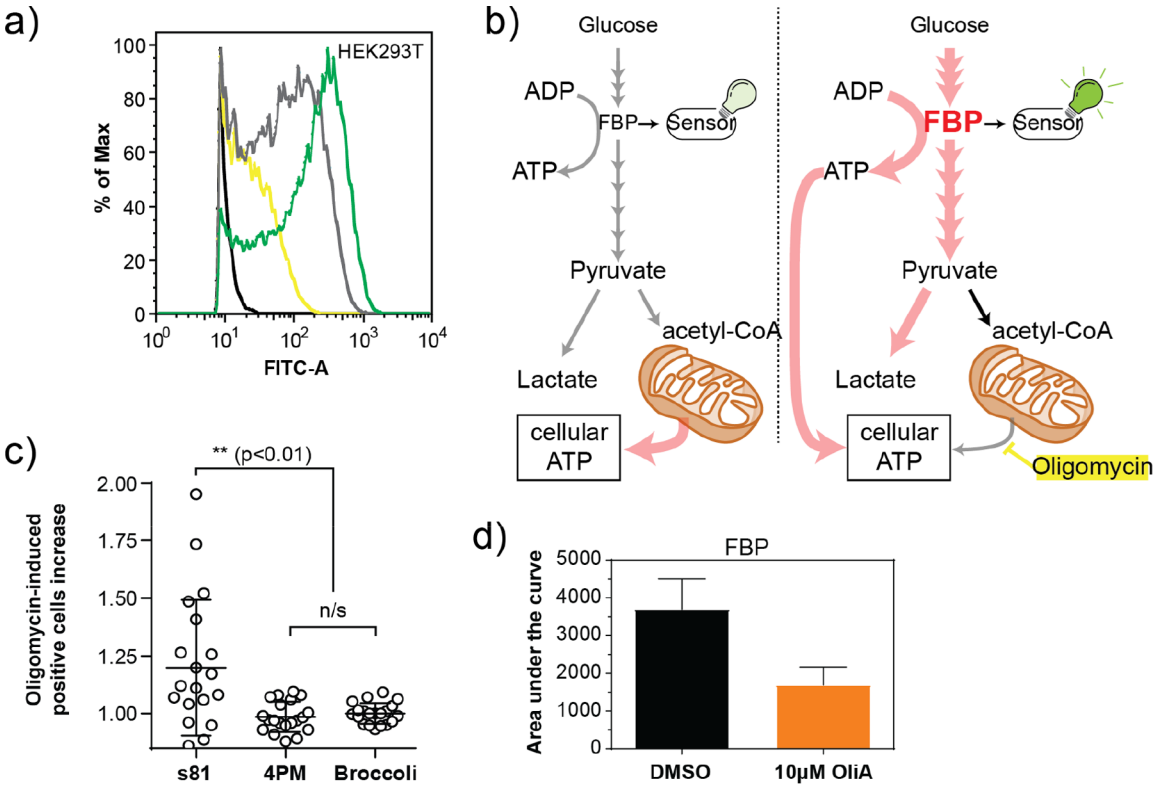

Figure 5. S81 detects oligomycin-induced variations in glycolytic flux independently from FBP. (a) Cytogram plot showing the population shift of HEK293T cells expressing the FBP sensor 81 (yellow) compared to 4PM (gray) and Broccoli (green). Cytograms were normalized to non-transfected cells, which were set to 1% (black). One representative experiment out of $n = 5$ is shown. (b) Schematic of the oligomycin A-induced glycolytic flux that increases intracellular FBP. Physiologically, ATP production is assigned to oxidative phosphorylation, based in the mitochondria, and the ATP production associated with glycolysis is negligible. Once treated with oligomycin A, oxidative phosphorylation is abolished and the ATP burden is shunted to glycolysis, which boosts glycolytic flux and intracellular FBP. (c) Discrimination of the oligomycin-induced glycolytic flux boost in HEK293T cells expressing sensor 81 compared to 4PM and Broccoli RNAs. The oligomycin-induced positive cell increase was calculated by dividing each treated value for each untreated value inside one experiment. Data represent $n = 5$ independent experiments, two of which were done in a blinded manner. *P*-values were calculated using the Mann−Whitney non-parametric test. (d) Intracellular FBP level decreased in HEK293T cells treated with oligomycin A (OliA) compared to the solvent alone (DMSO). Extracted ion chromatograms of FBP were determined by LC−MS, and the relative intensities are presented as the area under the curve (mean ± SEM from two independent experiments).

the integration within the scaffold (Supporting Information, Figure 13). Then, s81 embedded in the scaffold was expressed in HEK293T with the 4PM mutant as a control RNA and Broccoli, another DFHBI-binding aptamer previously used to establish the Tornado expression system.[29] Importantly, the fluorescence discrepancy of s81 and 4PM as cellular RNA (Figure 5a) reflected the response behavior observed in vitro (Figure 4d).

Seminal studies indicated that the level of FBP mirrors the glycolytic state of a cell.[3,17] To validate if s81 senses changes in the FBP concentration, we measured the sensor's fluorescence in cells treated or untreated with the antibiotic oligomycin. Oligomycin is used to measure the maximum glycolytic reserve in mammalian cell lines.[3,17,18] Upon oligomycin treatment, ATP production through the oxidative phosphorylation in mitochondria is inhibited, leading to an increase in glycolysis and hence FBP production (Figure 5d). We transfected HEK293T cells with s81, 4PM control (Figure 5c), and Broccoli RNA to measure the oligomycin-induced fluorescence increase, which was compared to the untreated sample. In the presence of oligomycin, cells expressing s81 showed an increased fluorescence signal, whereas the DFHBI fluorescence of cells expressing Broccoli or PM4 remained unchanged (Figure 5c). The specific response of s81 to oligomycin treatment indicated that this engineered RNA could be applied as a molecular tool to measure changes in the glycolytic flux in HEK293T cells.

Next, we quantified the relative level of FBP and other glycolytic intermediates in HEK293T cells treated by oligomycin A or DMSO by LC−MS. Tanner and co-workers correlated FBP levels with oligomycin-induced glycolytic boost in iBMK cells,[3,17] and thus, oligomycin concentration, cell handling, and metabolite extraction strictly followed the described protocol but were applied in HEK293T cells instead. In contrast to iBMK cells, FBP levels decreased when HEK293T cells were treated with oligomycin (Figure 5d). A similar trend was observed for F6P and Glc6P (Supporting Information, Figure 14), glycolytic precursor molecules of FBP that cross-reacted in the specificity assay for s81 (Figure 4e). The flow cytometry results exhibiting the s81 fluorescence response to oligomycin were thus repeated head-to-head with the intracellular quantification of FBP, measured with an orthogonal enzymatic kit quantification method to cross-validate the results obtained by LC−MS. Again, s81 but not 4PM or Broccoli controls responded to oligomycin, but FBP levels were shown to decrease upon oligomycin treatment (Supporting Information, Figure 15). Taken together, these results indicated that s81 showed promise to detect glycolytic

https://doi.org/10.1021/acschembio.2c00100
ACS Chem. Biol. 2022, 17, 1164−1173

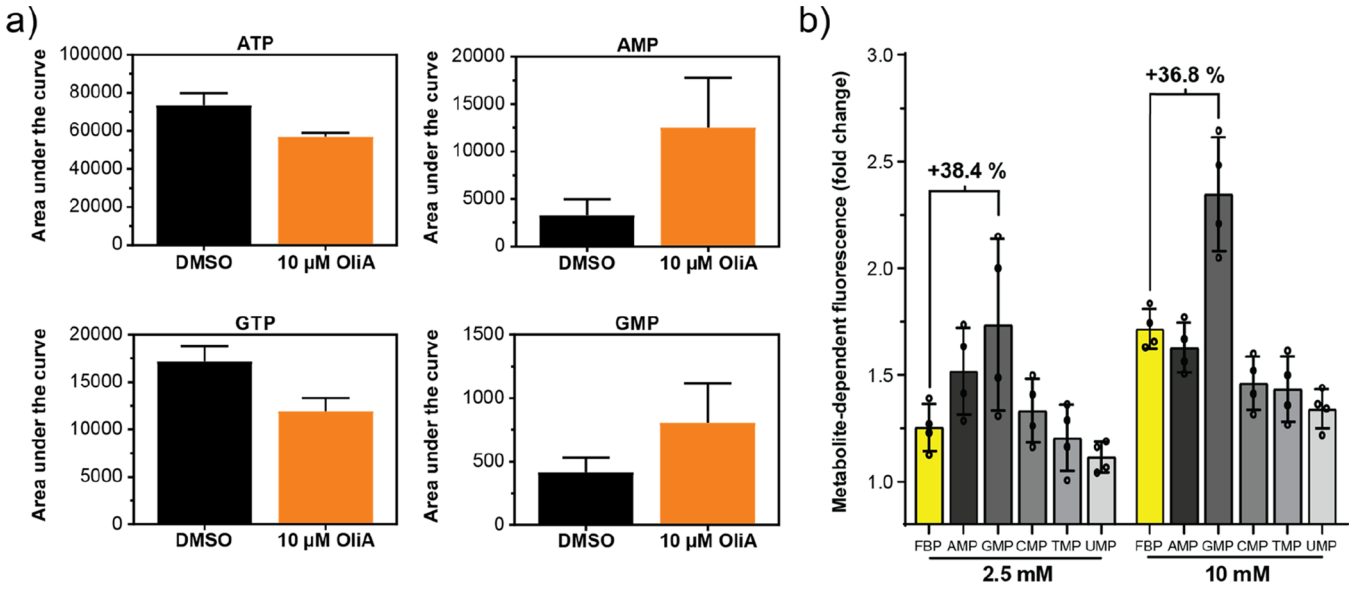

Figure 6. S81 robustly responds to GMP that was found to increase intracellularly upon oligomycin A treatment. (a) Intracellular ATP, AMP, GTP, and GMP levels in HEK293T cells treated with oligomycin A (OliA) or the solvent alone (DMSO) were determined by LC−MS analysis and are presented as relative intensities (area under the curve, mean ± SEM from two independent experiments). (b) Fluorescence response of s81 to a panel of monophosphate nucleotides AMP, GMP, CMP, TMP, and UMP compared to FBP. Data were normalized to the unspecific fluorescence variation of aptamer D1 with the different ligands at the given concentration, which was set to 1. The fluorescence readout was measured at 1 μM RNA and 10 μM DFHBI in 40 mM Tris-HCl pH 7.9, 50 mM KCl, and 30 mM $MgCl_2$.

variations—such as in response to oligomycin—but its cellular target is likely a different glycolytic intermediate, but FBP, responding to oligomycin in HEK293T cells.

The concentration of adenosine monophosphate (AMP) increases upon oligomycin treatment, mainly due to the enhanced AMPK activity.[30] This evidence was also confirmed by our LC−MS analysis, where AMP levels in oligomycin A-treated HEK293T cells were threefold higher compared to the DMSO control (AMP, Figure 6a). Similar results were observed for guanosine monophosphate (GMP, Figure 6a). Conversely, ATP and GTP were shown to decrease in the oligomycin-treated samples (Figure 6a). Consequently, we tested a panel of mono-phosphorylated nucleotides for their capability to elicit s81 response in vitro (Figure 6b). These experiments revealed GMP triggering s81 responses and, of note, to a higher extent when compared to FBP-induced fluorescence (+36−38%, Figure 6b).

In conclusion, we developed and characterized an RNA-based fluorescence sensor, named s81, which responded to variations in FBP in vitro and could qualitatively probe the increase in the glycolytic flux caused by oligomycin, a widely applied glycolytic booster. Contrary to the literature, however, we found FBP not to correlate with the oligomycin-driven glycolytic flux, whereas mono-phosphorylated nucleotides such as AMP and GMP did. To note, s81 showcased a response to GMP that outclassed even that of FBP, possibly indicating that its cellular response to oligomycin might be due to GMP. Other metabolite targets elicited s81 fluorescence to a different degree, and many signals might work in concert for the end-point response to arise. Likewise, and because the sensor's performance was found to be dependent on ion composition and concentration, fluctuations of ions might also undermine s81's cellular fluorogenic properties upon oligomycin treatment.

S81 was obtained by grafting the FBP-responsive aptamer C45[24] into the scaffold of the Spinach fluorogenic RNA.[23] Recently, Ortega et al. have grafted the C45 aptamer into the hammerhead ribozyme sequence to obtain a ribozyme switch that responded ratiometrically to the intracellular FBP increase in *Saccharomyces cerevisiae*,[24] thus validating the applicability of C45 as an FBP-responsive module. S81 was identified by a μIVC-based approach, while conventional in vitro selection was incapable of enriching the library accordingly. This finding illustrates the advantage of functional screening-based selection (using fluorescence here) compared to affinity enrichment. We employed a library design inspired by natural riboswitches that rely on nucleotide stretch sequestration, previously used to convert a natural TPP-sensing riboswitch into a TPP fluorogenic biosensor.[15] The present work reports on the first application of this concept to a completely synthetic aptamer and is an important stepping stone to fields like bioengineering and synthetic biology. This design is appealing and opens a route to be combined with efficient selection methods, thereby gaining RNA aptamer domains binding to metabolites and in which the stretch sequestration design is already reflected, for example, capture-SELEX approaches. This methodology would enable a generalizable procedure for the rapid identification of fluorogenic RNA-based biosensors going beyond current limitations of rational-based design and testing strategies. Fortunately, this approach will be combinable with other yet-to-be-generated light-up RNAs that have broader and wavelength-shifted fluorescence properties excellently suited for cellular and in vivo applications.

METHODS

μIVC Screening. The microfluidic chip development and the droplet digital PCR preparation followed the protocol from Autour et al.[21] However, the droplet occupancy was fine-tuned in the first screening cycle to accommodate a higher variability, increasing the initial droplet occupancy of the ddPCR to an occupancy of 65% (λ = 1) and screening for more than 5 million droplets. Occupancy was decreased in cycles 2 and 3, accounting for 17 and 27%, respectively.

https://doi.org/10.1021/acschembio.2c00100
ACS Chem. Biol. 2022, 17, 1164−1173

The ddPCR emulsion (made of 2.5 pL droplets) was PCR-amplified off-chip. Then, each thermocycled PCR droplet was fused 1 to 1 with a droplet containing an in vitro transcription (IVT) mixture supplemented with FBP for a final concentration of 2.5 mM for the first two positive screening cycles, while in the third cycle, FBP was omitted. The IVT mix contained 2 mM NTPs, 25 mM $MgCl_2$, 40 mM Tris-HCl pH 7.9, 50 mM KCl, 5 mM DTT, 1 mM spermidine, 0.1% Pluronic F68, 1 μL PPase, 20 μM DFHBI-1T, 0.5 μM Dextran-Texas Red, and 0.5 U μL^{-1} T7 RNA polymerase. The IVT mix was kept on ice during the droplet fusion; the emulsion was collected off-chip in a tube and incubated for 1 h at 37 °C to allow RNA transcription to occur. Droplet sorting was carried out by re-injecting the emulsion on a microfluidic sorting device designed to analyze the green (DFHBI-1T) and orange (Texas Red) fluorescence of each droplet. Cycles 1 and 2 of positive screening were performed in the presence of 2.5 mM FBP, and the top greenest droplets—0.02% and 0.46%, respectively—displaying an orange fluorescence corresponding to single fused droplets were gated. Next, cycle 3 negative screening was performed in the absence of FBP, and gates were screened for nil (4%), dim (4%), and highly fluorogenic (2.6%) droplets with an orange fluorescence corresponding to single fused droplets. In both screening conditions, gated droplets were deflected into the collection channel by applying an AC field (1000 V 30 kHz) and collected off-chip. Finally, the sorted droplets were treated with 100 μL 1*H*,1*H*,2*H*,2*H*-perfluoro-1-octanol to break the emulsion by vortexing, and the DNA-containing aqueous phase was retrieved.

In Vitro Fluorescence Measurements. In all in vitro fluorescence assays, the RNA—either library or synthesized single sequence—was purified by Urea-PAGE gel followed by the crush-soak method and was fixed at a concentration of 1 μM. The fluorophore used was DFHBI at a concentration of 10 μM, while it was substituted for its enhanced variant DFHBI-1T for screening and cellular application. The end-point fluorescence value was used as a proxy of the formation of the RNA-fluorophore complex. The initial sensor candidate shortlisting was performed in a selection medium (2 mM NTP, 25 mM $MgCl_2$, 50 mM KCl, 5 mM DTT, 1 mM spermidine, 0.1% of pluronic F68, and 1 μL PPase in 40 mM Tris-HCl pH 7.9), while all the other assays were performed in minimal fluorescence buffer (50 mM KCl in 40 mM Tris-HCl pH 7.9) with a concentration of $MgCl_2$ dependent on the concentration of FBP in that assay. For EC_{50} determination, the affinity curves in the presence and absence of FBP were determined using nonlinear regression analysis in Prism software and matched by least-squares fitting to a standard dose−response model for 1:1 complexation. Values represent the mean of three independent experiments ±1 standard deviation. Fluorescence emission was recorded using EnSpire Multimode Plate Reader (PerkinElmer) with the following instrument parameter: excitation wavelength, 462 nM; emission wavelength, 503 nM; slit widths, 1 nM. Fluorescence intensity was measured as relative fluorescence units (RFU)

Cell Culture and Transfection. HEK293T (ATCC CRL-3216) cells were maintained in DMEM, supplemented with 10% FBS, 100 U mL^{-1} penicillin, and100 mg mL^{-1} streptomycin solution under standard tissue culture conditions. All cells were split using TrypLE Express according to the manufacturer's instructions. Cell lines were plated in a 24-well TC plate and transfected with FuGENE using the Opti-MEM I Reduced Serum Media to resuspend the vector. To promote HEK293T adhesion, the plate was treated with Poly-L-Lysine solution for 1 h and washed with D-PBS. For HEK293T cells, 5×10^4 cells were seeded per well and transfected with a 25 μL Opti-MEM solution containing 500 ng and 1.5 μL transfection reagent per well. Cells were transfected 24 h after seeding. Two days after transfection, HEK293T cells were detached with TrypLE, diluted with DMEM 10% FBS, and centrifuged at 200 rcf for 5 min. The cellular pellet was resuspended in DMEM 10% FBS containing 40 μM DFHBI-1T and kept on ice until analysis. Cells were analyzed using FACS Canto II (BD Bioscience). Plots were generated using FlowJo software v9.6.3.

Oligomycin A Treatment. Analogous to the construct comparison, HEK293T cells were seeded on a 24-well plate in DMEM 10% FBS and transfected the next day. Two days after transfection, the cell medium was switched to a formulated DMEM (1 g L^{-1} glucose, 10% FBS) containing 2 mM glutamine, added shortly before the assay. The formulated medium was prepared according to the manufacturer's instructions for powdered DMEM. For positive cells, the cell medium was supplemented with 10 μM oligomycin A for 30 min. Cells were detached with TrypLE, diluted with the corresponding DMEM formulation, and centrifuged at 200*g* for 5 min at 4 °C. The cellular pellet was resuspended in the corresponding DMEM formulation containing 40 μM DFHBI-1T and kept on ice until analysis. Cells were gated and normalized analogous to the construct comparison. The oligomycin assay was repeated in a double-blind setting to ensure non-biased sample treatment. Samples were prepared for transfection and handed out to a second investigator for relabeling. Samples were transfected, and the oligomycin assay was performed according to the protocol. After flow cytometry measurement, the sample blinding was unveiled.

Metabolite Extraction and LC−MS Quantification. The metabolite extraction followed strictly the protocol described by Park et al.[17] Culture dishes of 150 cm^2 (734−2322, VWR) were treated with a poly-lysine solution (20 mL per plate) for 1 h and then washed twice with DPBS and kept under the hood to dry up. 6×10^6 HEK293T cells were seeded in each plate and cultivated for 48 h in formulated DMEM (1 g/L glucose, 2 mM glutamine, 10% FBS). Three dishes were seeded for each condition: oligomycin (treated), DMSO (untreated), pre-spiked control, post-spiked control. One dish was used for cell counting, whereas 2 dishes were subjected to metabolite extraction. After 48 h growth, cells were treated with a fresh formulated medium containing oligomycin (10 μM) or DMSO vehicle (untreated) for 30 min. Pre-spiked and post-spiked controls were also treated with DMSO. Subsequently, cell metabolism was quenched by placing the cell dishes on a −20 °C metal block and the respective metabolite extraction protocol. Mammalian cell metabolism was quenched, and metabolites were extracted by quickly aspirating media from culture dishes and adding cold (−20 °C) 80:20 methanol/water. The plates were placed at −20 °C for 20 min. Then, cells were scraped off the culture dish surface. Note that, in all cases, quenching was performed without any washing steps that can perturb the metabolism. The dishes were rinsed with an additional 15 mL of ice-cold ddH_2O, and the two suspensions were collected together and quenched in LN2. Before LN2 quenching, the pre-spiked control added a metabolite mixture (1 mM Glc6P, 1 mM F6P, and 1 mM FBP) of 400 μL. The samples were cleared from cellular debris by centrifugation (20 min at 4 °C, 4500*g*). At this point, also the post-spiked control solution was spiked with a metabolite mixture (1 mM Glc6P, 1 mM F6P, and 1 mM FBP) of 400 μL. The 30 mL solution containing the metabolite mixture was finally frozen at −80 °C, lyophilized, and stored at −80 °C. Lyophilized cell extracts were further solved in 300 μL water and cleared up by centrifugation on Amicon ultra 3K columns (Millipore, Cat #UFC500396). Then, 5 μL of the samples or of the 1 mM FBP was analyzed using an ESI-TOF mass spectrometer (micrO-TOF II, Bruker) operated in the negative ion mode (mass range 150−1000 m z^{-1}) and connected to an UltiMate 3000 high-performance liquid chromatography (HPLC) system (Dionex). For the FBP quantitative analysis, a previously described LC−MS protocol, optimized for nucleotide quantification using a SeQuant ZIC-pHILIC column, was applied.[31] The quantification of the isomeric sugar phosphates Glc6P and F6P was performed using an alternative LC−MS protocol, optimized for the separation of phosphorylated saccharides. Briefly, elution occurred with a flow rate of 0.3 mL min^{-1} using isocratic flow with an eluent 25 mM $HCOONH_4$ in Millipore water: CH_3CN (80:20) over 15 min. The column HILICpak VT-50 2D (Shodex) was used for separation, and the temperature was set to 60 °C. The MS protocol was the same, as used for the quantification of FBP. Interestingly, with this separation, we were not able to detect FBP or nucleotides containing two or three phosphates on the HILICpak VT-50 2D column under the run conditions. Data Analysis program (Bruker) was used to present the masses as extracted-ion chromatograms for FBP (338.989 m z^{-1}), Glc6P (259.022 m z^{-1}), F6P (259.022), ATP (505.989 m z^{-1}), AMP (346.056 m z^{-1}), GTP (521.983 m z^{-1}), and GMP

https://doi.org/10.1021/acschembio.2c00100
ACS Chem. Biol. 2022, 17, 1164−1173

(362.051 m z^{-1}), and the peak areas were calculated and quantified with Prism 8 (GraphPad). The retention times of the investigated metabolites were verified by including 1 mM standards of the above-indicated metabolites.

■ ASSOCIATED CONTENT

Supporting Information

The Supporting Information is available free of charge at https://pubs.acs.org/doi/10.1021/acschembio.2c00100.

Additional methods, materials, and sequence tables; SELEX and NGS analysis results; μIVC screening; sequence characterization; and LC−MS analysis (PDF)

■ AUTHOR INFORMATION

Corresponding Author

Günter Mayer − *Life and Medical Sciences Institute (LIMES), University of Bonn, 53121 Bonn, Germany; Center of Aptamer Research & Development, University of Bonn, 53121 Bonn, Germany;* orcid.org/0000-0003-3010-4049; Email: gmayer@uni-bonn.de

Authors

Ignazio Geraci − *Life and Medical Sciences Institute (LIMES), University of Bonn, 53121 Bonn, Germany*

Alexis Autour − *Université de Strasbourg, CNRS, Architecture et Réactivité de l'ARN, UPR 9002, 67084 Strasbourg, France*

Georg Pietruschka − *Life and Medical Sciences Institute (LIMES), University of Bonn, 53121 Bonn, Germany*

Aleksandra Shiian − *Life and Medical Sciences Institute (LIMES), University of Bonn, 53121 Bonn, Germany*

Marina Borisova − *Interfaculty Institute of Microbiology and Infection Medicine, Organismic Interactions/Glycobiology, Eberhard Karls University of Tübingen, 72076 Tübingen, Germany*

Christoph Mayer − *Interfaculty Institute of Microbiology and Infection Medicine, Organismic Interactions/Glycobiology, Eberhard Karls University of Tübingen, 72076 Tübingen, Germany;* orcid.org/0000-0003-4731-4851

Michael Ryckelynck − *Université de Strasbourg, CNRS, Architecture et Réactivité de l'ARN, UPR 9002, 67084 Strasbourg, France;* orcid.org/0000-0002-2225-3733

Complete contact information is available at: https://pubs.acs.org/10.1021/acschembio.2c00100

Notes

The authors declare no competing financial interest.

■ ACKNOWLEDGMENTS

We thank members of the Mayer and Ryckelynck laboratories for assistance with experiments. We thank the laboratory of Jaffrey at the Cornell University for providing the Tornado plasmids used for cloning and expression of the sensor system in mammalian cells. This work was supported by funds from the European Union (642738 MetaRNA H2020-MSCA-ITN-2014GRANTS), ERC ("OptoRibo", 615381), and the Deutsche Forschungsgemeinschaft (German Research Foundation) Project-ID 398967434—TRR261 to G.M. and to C.M. and SFB1089 to G.M. This work received financial support from Agence Nationale de la Recherche (BrightRiboProbes, ANR-16-CE11-0010-01) to M.R. It also has been published under the framework of the LabEx: ANR-10-LABX-0036_NETRNA (M.R.) and benefits from a funding from the state managed by the French National Research Agency as part of the Investments for the Future program. It was also supported by the Université de Strasbourg and the Centre National de la Recherche Scientifique.

■ REFERENCES

(1) Folly, B. B.; Ortega, A. D.; Hubmann, G.; Bonsing-Vedelaar, S.; Wijma, H. J.; van der Meulen, P.; Milias-Argeitis, A.; Heinemann, M. Assessment of the interaction between the flux-signaling metabolite fructose-1,6-bisphosphate and the bacterial transcription factors CggR and Cra. *Mol. Microbiol.* **2018**, *109*, 278−290.

(2) Monteiro, F.; Hubmann, G.; Takhaveev, V.; Vedelaar, S. R.; Norder, J.; Hekelaar, J.; Saldida, J.; Litsios, A.; Wijma, H. J.; Schmidt, A.; et al. Measuring glycolytic flux in single yeast cells with an orthogonal synthetic biosensor. *Mol. Syst. Biol.* **2019**, *15*, No. e9071.

(3) Tanner, L. B.; Goglia, A. G.; Wei, M. H.; Sehgal, T.; Parsons, L. R.; Park, J. O.; White, E.; Toettcher, J. E.; Rabinowitz, J. D. Four Key Steps Control Glycolytic Flux in Mammalian Cells. *Cell Syst.* **2018**, *7*, 49−62.

(4) Specht, E. A.; Braselmann, E.; Palmer, A. E. A Critical and Comparative Review of Fluorescent Tools for Live Cell Imaging. *Annu. Rev. Physiol.* **2017**, *79*, 93−117.

(5) Ying, Z.-M.; Wu, Z.; Tu, B.; Tan, W.; Jiang, J.-H. Genetically Encoded Fluorescent RNA Sensor for Ratiometric Imaging of MicroRNA in Living Tumor Cells. *J. Am. Chem. Soc.* **2017**, *139*, 9779−9782.

(6) Strack, R. L.; Jaffrey, S. R. New approaches for sensing metabolites and proteins in live cells using RNA. *Curr. Opin. Chem. Biol.* **2013**, *17*, 651−655.

(7) Sun, Z.; Nguyen, T.; McAuliffe, K.; You, M. Intracellular Imaging with Genetically Encoded RNA-based Molecular Sensors. *Nanomaterials* **2019**, *9*, 233.

(8) Wang, X. C.; Wilson, S. C.; Hammond, M. C. Next-generation RNA-based fluorescent biosensors enable anaerobic detection of cyclic di-GMP. *Nucleic Acids Res.* **2016**, *44*, No. e139.

(9) You, M.; Litke, J. L.; Wu, R.; Jaffrey, S. R. Detection of Low-Abundance Metabolites in Live Cells Using an RNA Integrator. *Cell Chem. Biol.* **2019**, *26*, 471−481.

(10) Kim, H.; Jaffrey, S. R. A Fluorogenic RNA-Based Sensor Activated by Metabolite-Induced RNA Dimerization. *Cell Chem. Biol.* **2019**, *26*, 1725−1731.

(11) Mieczkowski, M.; Steinmetzger, C.; Bessi, I.; Lenz, A.-K.; Schmiedel, A.; Holzapfel, M.; Lambert, C.; Pena, V.; Höbartner, C. Large Stokes shift fluorescence activation in an RNA aptamer by intermolecular proton transfer to guanine. *Nat. Commun.* **2021**, *12*, 3549.

(12) Paige, J. S.; Wu, K. Y.; Jaffrey, S. R. RNA Mimics of Green Fluorescent Protein. *Science* **2011**, *333*, 642−646.

(13) Wirth, R.; Gao, P.; Nienhaus, G. U.; Sunbul, M.; Jäschke, A. SiRA: A Silicon Rhodamine-Binding Aptamer for Live-Cell Super-Resolution RNA Imaging. *J. Am. Chem. Soc.* **2019**, *141*, 7562−7571.

(14) Bouhedda, F.; Fam, K. T.; Collot, M.; Autour, A.; Marzi, S.; Klymchenko, A.; Ryckelynck, M. A dimerization-based fluorogenic dye-aptamer module for RNA imaging in live cells. *Nat. Chem. Biol.* **2020**, *16*, 69−76.

(15) You, M.; Litke, J. L.; Jaffrey, S. R. Imaging metabolite dynamics in living cells using a Spinach-based riboswitch. *Proc. Natl. Acad. Sci.* **2015**, *112*, E2756−E2765.

(16) Kellenberger, C. A.; Wilson, S. C.; Sales-Lee, J.; Hammond, M. C. RNA-Based Fluorescent Biosensors for Live Cell Imaging of Second Messengers Cyclic di-GMP and Cyclic AMP-GMP. *J. Am. Chem. Soc.* **2013**, *135*, 4906−4909.

(17) Park, J. O.; Tanner, L. B.; Wei, M. H.; Khana, D. B.; Jacobson, T. B.; Zhang, Z.; Rubin, S. A.; Li, S. H.-J.; Higgins, M. B.; Stevenson, D. M.; et al. Near-equilibrium glycolysis supports metabolic homeostasis and energy yield. *Nat. Chem. Biol.* **2019**, *15*, 1001−1008.

(18) Winer, L. S. P.; Wu, M. Rapid Analysis of Glycolytic and Oxidative Substrate Flux of Cancer Cells in a Microplate. *PLoS One* **2014**, *9*, No. e109916.
(19) Warner, K. D.; Chen, M. C.; Song, W.; Strack, R. L.; Thorn, A.; Jaffrey, S. R.; Ferré-D'Amaré, A. R. Structural basis for activity of highly efficient RNA mimics of green fluorescent protein. *Nat. Struct. Mol. Biol.* **2014**, *21*, 658−663.
(20) Baret, J.-C.; Miller, O. J.; Taly, V.; Ryckelynck, M.; El-Harrak, A.; Frenz, L.; Rick, C.; Samuels, M. L.; Hutchison, J. B.; Agresti, J. J.; et al. Fluorescence-activated droplet sorting (FADS): efficient microfluidic cell sorting based on enzymatic activity. *Lab Chip* **2009**, *9*, 1850−1858.
(21) Autour, A.; Westhof, E.; Ryckelynck, M. iSpinach: a fluorogenic RNA aptamer optimized for in vitro applications. *Nucleic Acids Res.* **2016**, *44*, 2491−2500.
(22) Tuerk, C.; Gold, L. Systematic Evolution of Ligands by Exponential Enrichment: RNA Ligands to Bacteriophage T4 DNA Polymerase. *Science* **1990**, *249*, 505−510.
(23) Okuda, M.; Fourmy, D.; Yoshizawa, S. Use of Baby Spinach and Broccoli for imaging of structured cellular RNAs. *Nucleic Acids Res.* **2017**, *45*, 1404−1415.
(24) Long, Y.; Pfeiffer, F.; Mayer, G.; Schrøder, T. D.; Özalp, V. C.; Olsen, L. F. Selection of Aptamers for Metabolite Sensing and Construction of Optical Nanosensors. *Methods Mol. Biol.* **2016**, *1380*, 3−19.
(25) Ortega, A. D.; Takhaveev, V.; Vedelaar, S. R.; Long, Y.; Mestre-Farràs, N.; Incarnato, D.; Ersoy, F.; Olsen, L. F.; Mayer, G.; Heinemann, M. A synthetic RNA-based biosensor for fructose-1,6-bisphosphate that reports glycolytic flux. *Cell Chem. Biol.* **2021**, *28*, 1554.
(26) Autour, A.; Bouhedda, F.; Cubi, R.; Ryckelynck, M. Optimization of fluorogenic RNA-based biosensors using droplet-based microfluidic ultrahigh-throughput screening. *Methods* **2019**, *161*, 46−53.
(27) Matsumura, S.; Kun, Á.; Ryckelynck, M.; Coldren, F.; Szilágyi, A.; Jossinet, F.; Rick, C.; Nghe, P.; Szathmáry, E.; Griffiths, A. D. Transient compartmentalization of RNA replicators prevents extinction due to parasites. *Science* **2016**, *354*, 1293−1296.
(28) Bailey, T. L.; Boden, M.; Buske, F. A.; Frith, M.; Grant, C. E.; Clementi, L.; Ren, J.; Li, W. W.; Noble, W. S. MEME Suite: tools for motif discovery and searching. *Nucleic Acids Res.* **2009**, *37*, W202−W208.
(29) Litke, J. L.; Jaffrey, S. R. Highly efficient expression of circular RNA aptamers in cells using autocatalytic transcripts. *Nat. Biotechnol.* **2019**, *37*, 667−675.
(30) Plaideau, C.; Liu, J.; Hartleib-Geschwindner, J.; Bastin-Coyette, L.; Bontemps, F.; Oscarsson, J.; Hue, L.; Rider, M. H. Overexpression of AMP-metabolizing enzymes controls adenine nucleotide levels and AMPK activation in HEK293T cells. *Faseb. J.* **2012**, *26*, 2685−2694.
(31) Gratani, F. L.; Horvatek, P.; Geiger, T.; Borisova, M.; Mayer, C.; Grin, I.; Wagner, S.; Steinchen, W.; Bange, G.; Velic, A.; et al. Regulation of the opposing (p)ppGpp synthetase and hydrolase activities in a bifunctional RelA/SpoT homologue from Staphylococcus aureus. *PLoS Genet.* **2018**, *14*, No. e1007514.

https://doi.org/10.1021/acschembio.2c00100
ACS Chem. Biol. 2022, 17, 1164−1173